

Visualizing band alignment across 2D/3D perovskite heterointerfaces of solar cells with light-modulated scanning tunneling microscopy

Po-Cheng Huang^{a,b,1}, Shao-Ku Huang^{c,1}, Ting-Chun Lai^c, Min-Chuan Shih^b, Hung-Chang Hsu^b, Chun-Hsiang Chen^b, Cheng-Chieh Lin^{d,e}, Chun-Hao Chiang^c, Chi-Ying Lin^c, Kazuhito Tsukagoshi^f, Chun-Wei Chen^{c,g,*}, Ya-Ping Chiu^{b,g,**}, Shiow-Fon Tsay^a, Ying-Chiao Wang^{f,***}

^a Department of Physics, National Sun Yat-sen University, Kaohsiung 80424, Taiwan

^b Department of Physics, National Taiwan University, Taipei 10617, Taiwan

^c Department of Materials Science and Engineering, National Taiwan University, Taipei 10617, Taiwan

^d International Graduate Program of Molecular Science and Technology (NTU-MST), National Taiwan University, Taipei 10617, Taiwan

^e Molecular Science and Technology Program, Taiwan International Graduate Program (TIGP), Academia Sinica, Taipei 11529, Taiwan

^f International Center for Young Scientists (ICYs) and WPI International Center for Materials Nanoarchitectonics (WPI-MANA), National Institute for Materials Science (NIMS), Tsukuba, Ibaraki 305-0044, Japan

^g Center of Atomic Initiative for New Materials (AI-MAT), National Taiwan University, Taipei 10617, Taiwan



ARTICLE INFO

Keywords:

Perovskite solar cells
2D/3D perovskite
Interface
Band mapping
Scanning tunneling microscopy

ABSTRACT

Graded 2D perovskite capping shells with continuously upshifting valence bands, produced by tailored dimensional engineering, can effectively extract holes from 3D perovskite cores. Real-space observation of electronic structures will fully reveal the operating mechanisms of 2D/3D hybrid perovskite solar cells (PSCs). Here, for the first time, light-modulated scanning tunneling microscopy visualizes the cross-sectional band alignment across 2D ($\text{C}_4\text{H}_9\text{NH}_3)_2(\text{CH}_3\text{NH}_3)_{n-1}\text{Pb}_n\text{I}_{3n+1}$)/3D $\text{CH}_3\text{NH}_3\text{PbI}_3$ stacked perovskites. By systematically analyzing their electronic configuration, the mixed-dimensional perovskite band structure along the vertical 3D-to-2D direction can be spatially resolved. Remarkably, the electric field in the 2D perovskite is larger under light illumination than under dark conditions, resulting in an increase in the concentration of holes and electrons distributed in the 2D and 3D perovskites, respectively. Benefiting from this electronic reconstruction, charge recombination is suppressed, thereby significantly promoting the 2D/3D PSC performance. Moreover, our method opens an avenue for direct, local mapping of optoelectronic device energy levels.

1. Introduction

Due to the extraordinary and continuously improving photophysical properties of organometal halide perovskite-based light harvesters, including the adjustable bandgap, high absorptivity and long-range balanced exciton diffusion lengths [1–8], the power conversion efficiencies (PCEs) of perovskite solar cells (PSCs) have gradually increased from 3.8% [9] to over 25% [10]. Despite this significant progress, the intrinsic instability of organic-inorganic three-dimensional (3D) perovskites in the ambient atmosphere remains unresolved [11,12].

Among the latest strategies, the formation of vertically aligned 2D/3D perovskite heterostructures has emerged as a feasible approach to slow down 3D perovskite degradation [5,13–22]. By incorporating large-sized spacer cations (e.g., aryl- [14–17,21] or alkylammonium [5, 18,19,22] salts) on 3D perovskites, Ruddlesden-Popper phase 2D perovskites will spontaneously grow on the topmost 3D segments through the reaction of long-chain organic cations with excess inorganic anions [22]. Owing to the hydrophobicity and notable chemical stability of long-chain cations [23–26] in 2D perovskite capping layers, 2D/3D PSCs show a substantially extended long-term lifetime compared to the

* Corresponding author at: Department of Materials Science and Engineering, National Taiwan University, Taipei 10617, Taiwan.

** Corresponding author at: Department of Physics, National Taiwan University, Taipei 10617, Taiwan.

*** Corresponding author.

E-mail addresses: chunwei@ntu.edu.tw (C.-W. Chen), ypchiu@phys.ntu.edu.tw (Y.-P. Chiu), steven7419082@gmail.com (Y.-C. Wang).

¹ P.-C. Huang and S.-K. Huang are equally contributed to this work.

<https://doi.org/10.1016/j.nanoen.2021.106362>

Received 22 June 2021; Received in revised form 16 July 2021; Accepted 19 July 2021

Available online 24 July 2021

2211-2855/© 2021 The Author(s). Published by Elsevier Ltd. This is an open access article under the CC BY license (<http://creativecommons.org/licenses/by/4.0/>).

air-sensitive 3D counterparts due to the blocking of the moisture penetration path. In addition to the stability, the open-circuit voltages (V_{OC}), fill factors (FFs) and overall PCEs of PSCs containing 2D/3D perovskite heterointerfaces are mostly boosted [5,14–16,19,20,22]. These performance augmentations are mainly ascribed to the existence of gradient energy levels in the dimensionally graded 2D perovskite layer [5,14,15]. After covering the 3D perovskite, the 2D perovskite film with upwardly shifting band edges easily extracts holes from the bottom 3D perovskite and further suppresses the interfacial electron-hole recombination, ultimately minimizing the energy loss inside 2D/3D PSCs. In brief, the improvement in photovoltaic parameters strongly depends on optimized band alignment. Furthermore, an in-depth study of the electronic environment across 2D/3D perovskite heterojunctions in real space is undoubtedly essential to promote device design. To date, only top-view conductive atomic force microscopy (c-AFM) has been used to attempt to probe the local electronic information of 2D/3D perovskite stacking-layered architectures [5,15]. However, three issues still prevent the comprehensive understanding of band architectures: (i) the c-AFM technique can only obtain the work function of a specific material based on the contact potential difference and not the complete energy band information; (ii) the surface measurement cannot account for the carrier transport behavior of vertical junctions; and (iii) analysis of the electronic structure after light soaking is missing. With these issues in mind, direct determination of the cross-sectional energy band structure around 2D/3D perovskites under light irradiation is thus desired.

Drawing on our previous experiments using scanning tunneling microscopy (STM) to image the vertical [27,28] and photoinduced [29] band alignments separately, here, we realize spatial visualization of valence bands (VBs) and conduction bands (CBs) across 2D/3D

perovskites by combining cross-sectional and light-modulation techniques in STM. By monitoring the band structure evolution based on light-modulated cross-sectional STM (LM-XSTM) results, flat and continuously upshifting bands can be mapped in the 3D and 2D regions along the 3D-to-2D direction, respectively. Moreover, upon optical excitation, the band bending at the 2D/3D perovskite heterointerface simultaneously increases, implying that more effective photocarrier separation occurs. This method offers visual reasons for the performance enhancements of 2D/3D PSCs and can in principle be extended to probe other semiconductor devices [30,31].

2. Experimental section

2.1. Structural determination of 2D/3D perovskites

To construct the 2D/3D perovskite stacking architecture, we first synthesized the 3D perovskite $\text{CH}_3\text{NH}_3\text{PbI}_3$ (MAPbI₃) matrix through an all-solution-processed deposition approach according to our procedures [32]. Next, an isopropanol solution containing 5 mM organic co-salts ($\text{CH}_3\text{NH}_3\text{I}$ (MAI) and $\text{C}_4\text{H}_9\text{NH}_3\text{I}$ (BAI)) was spin-coated onto the upper surface of 3D MAPbI₃ and then annealed at 70 °C for in situ growth of the 2D perovskite capping layer $(\text{BA})_2(\text{MA})_{n-1}\text{Pb}_n\text{I}_{3n+1}$ (where integer n is the layer number of inorganic lattices between BA cations). Fig. 1a depicts a high-resolution cross-sectional transmission electron microscopy (HRXTEM) image of an as-synthesized 2D/3D perovskite film. The distinct crystal fringes on the upper edge of the black region with an interplanar lattice distance of 3.24 Å can be assigned to the (0160) crystal plane of the 2D perovskite $(\text{BA})_2(\text{MA})_2\text{Pb}_3\text{I}_{10}$ (n = 3), whereas the thickness of the 2D perovskite layer is 8 ± 2 nm. In addition, other

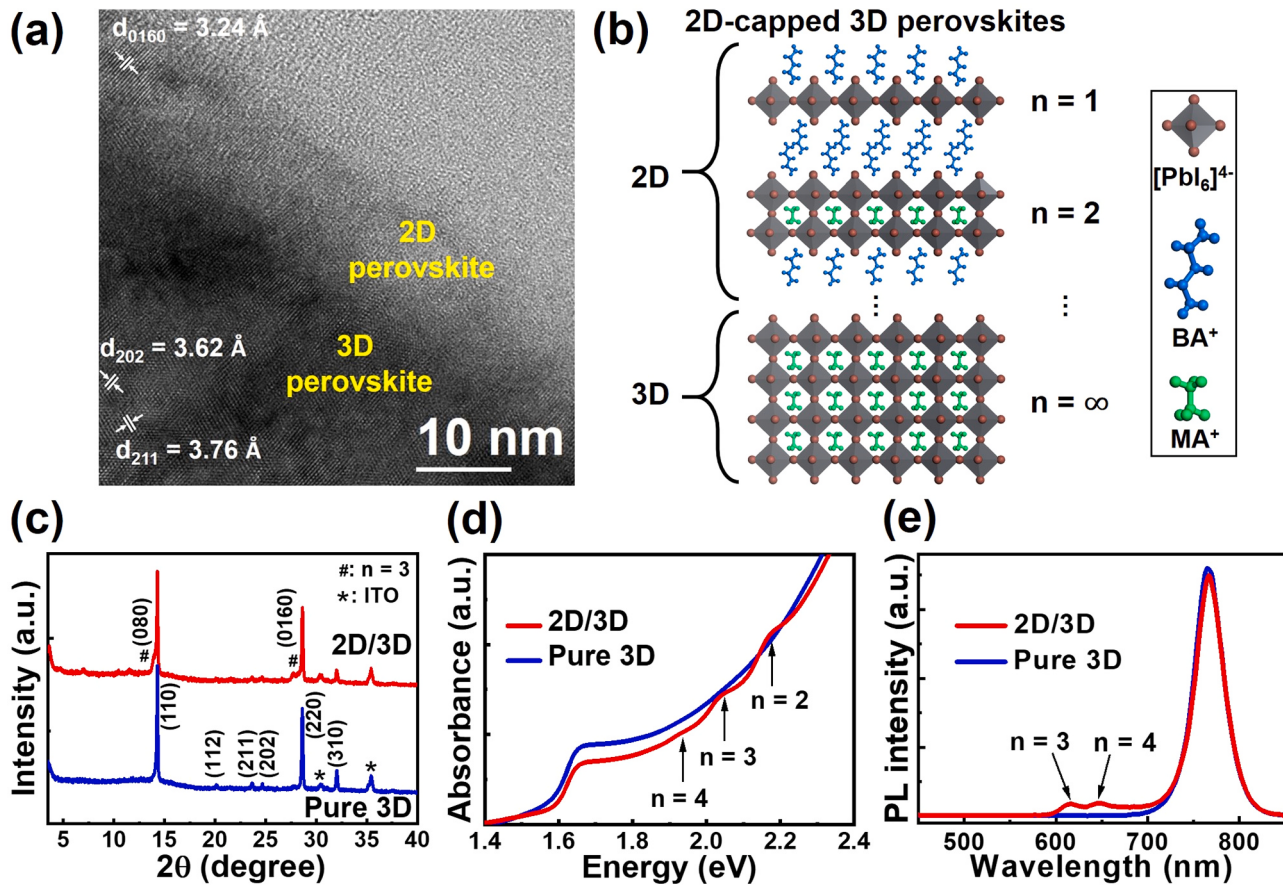


Fig. 1. 2D/3D perovskite heterostructure. (a) HRXTEM image of the 2D/3D perovskite heterostructure. (b) Schematic depiction of the proposed 2D $(\text{BA})_2(\text{MA})_{n-1}\text{Pb}_n\text{I}_{3n+1}$ /3D MAPbI₃ hybrid perovskite structure. (c) XRD patterns, (d) UV-vis absorption spectra and (e) PL spectra of the pure 3D perovskite film (blue line) and the 2D/3D hybrid perovskite film (red line).

fine fringes with two lattice spacings of 3.62 and 3.76 Å in the black region are found to match the 3D perovskite (202) and (211) facets, respectively, demonstrating successful growth of the 2D perovskite shell around the 3D perovskite core. The vertically stacked 2D/3D perovskite structure is schematically drawn in Fig. 1b. The continuously increasing n value from top to bottom in the 2D region can be understood in terms of the concentration gradient caused by the drop-casting process. During the isopropanol solution dripping treatment, the concentration of BA cations located near the 3D perovskite surface is higher than the internal concentration. Therefore, close to the surface, the total amount of BA integrated into interstitial sites of the corner-sharing $[PbI_6]^{4-}$ octahedral framework increases. As a result, the n values naturally increase from top to bottom within the 2D segment, which is also confirmed by previous reports [14,33]. To further verify 2D perovskites with various n values, the X-ray diffraction (XRD) patterns, UV-vis absorption spectra and steady-state photoluminescence (PL) spectra were successively analyzed. Fig. 1c displays the XRD measurements of 3D perovskites without and with the 2D perovskite capping layer. Compared with the pure 3D sample, the XRD pattern of the 2D/3D perovskite crystal has two additional peaks at 13.8° and 27.6°, which can be associated with the (080) and (0160) reflections of the 2D compound $(BA)_2(MA)_2Pb_3I_{10}$ ($n = 3$) [34,35], respectively, where the (0160) plane of the diffractogram is consistent with the observation of the 2D layer in the HRXTEM image (Fig. 1a). Moreover, the XRD peak intensities of MAPbI₃ in the 2D/3D perovskites are lower than those in the pure 3D perovskite

counterpart, demonstrating that some of the 3D crystal has been converted to 2D layered perovskites [5]. This transition can be further discussed based on the optical absorption spectra. As shown in Fig. 1d, the absorption feature in the photon energy range of 1.59–1.68 eV corresponds to the characteristic absorption band of the 3D MAPbI₃ perovskite crystal [36]. After the 2D/3D superlattice is formed, the absorption edge of MAPbI₃ is slightly decreased and sequentially replaced by new excitonic absorption peaks of the 2D perovskites at photon energies of 1.93 ($n = 4$), 2.03 ($n = 3$) and 2.17 eV ($n = 2$) [34,35]. These 2D crystal planes agree well with the magnified XRD result at low angles ($2\theta < 14^\circ$) (Fig. S1, Supporting Information). Furthermore, with the generation of the 2D phase, we observe two additional PL emission shoulders near 642 and 611 nm in Fig. 1e, corresponding to strong excitonic recombination radiation in the multiple quantum well-like 2D perovskites with $n = 4$ and 3 [34,35], respectively. All the results indicate the presence of gradual multidimensional 2D/3D hybrid perovskites with stacking order after BA cation treatment.

3. Results and discussion

3.1. Photovoltaic performance

To explore the potential impact of the 2D-capped 3D perovskite film on the solar cell performance, we prepared PSCs with the device structure indium tin oxide (ITO) anode/C₆₀ pyrrolidine tris-acid (CPTA)-

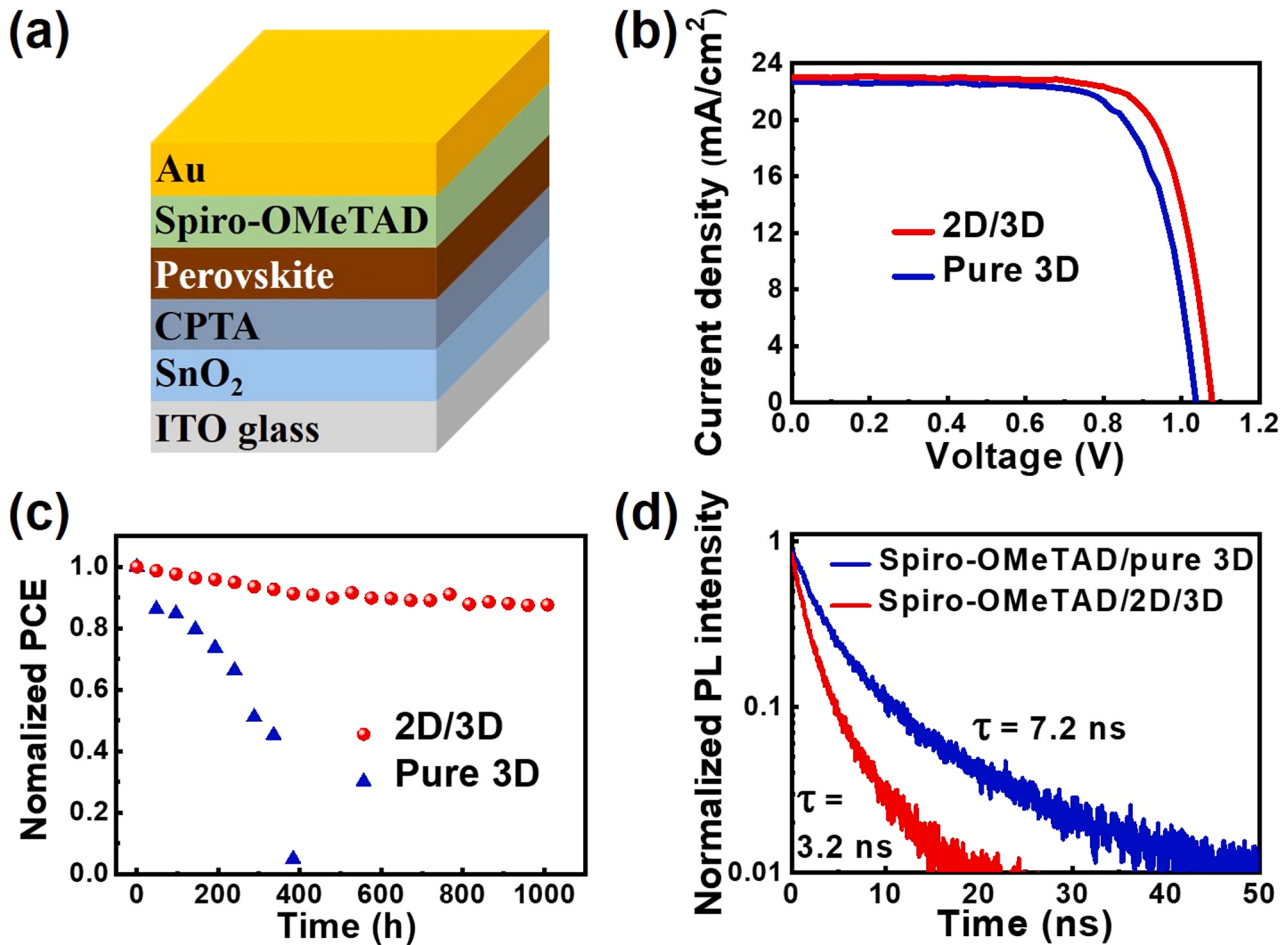


Fig. 2. Photovoltaic performances of the 2D/3D PSCs. (a) Schematic illustration of the PSC device architecture. (b) Reverse J-V scans of the champion pure 3D and 2D/3D PSC devices under AM 1.5 G illumination (100 mW cm⁻²). (c) Normalized PCE comparison of the long-term stability of the nonencapsulated pure 3D and 2D/3D PSC devices exposed to ambient atmospheric conditions (relative humidity $\approx 40\%$). (d) TRPL decay transient spectra of the glass/pure 3D perovskite/Spiro-OMeTAD and glass/2D/3D hybrid perovskite/Spiro-OMeTAD films. The PL emission is collected at 765 nm (that is, in the emission region of the 3D MAPbI₃ perovskite) under excitation at 466 nm.

passivated SnO_2 electron transport bilayer/3D perovskite/2D perovskite/2,2',7,7'-tetrakis-(N,N-di-p-methoxyphenylamine)-9,9'-spirobi-fluorene (Spiro-OMeTAD) hole transport layer/Au cathode, as illustrated in the cartoon in Fig. 2a. The corresponding cross-sectional TEM (XTEM) image of an as-fabricated PSC shows that the thickness of the 2D/3D hybrid perovskite photoactive layer is approximately 340 nm (Fig. S2, Supporting Information). The current density-voltage (J-V) plots of the PSCs under AM 1.5 G irradiation at 100 mW cm^{-2} before (hereafter referred to simply as “Pure 3D”) and after covering the 3D perovskite with a 2D capping layer (hereafter referred to simply as “2D/3D”) are presented in Fig. 2b. The champion 2D/3D PSC achieved a PCE of 19.2% with a V_{OC} of 1.08 V, an FF of 77.3% and a short-circuit current density (J_{SC}) of 23.02 mA cm^{-2} . In comparison, the PSC using the pure 3D perovskite as the light harvester showed significantly lower photovoltaic metrics, with a PCE of 17.1%, a V_{OC} of 1.03 V, an FF of 73.0% and a J_{SC} of 22.73 mA cm^{-2} . Additionally, statistical photovoltaic values based on 20 individual PSC devices indicate that the performance improvements after introducing 2D perovskites into MAPbI_3 -based PSCs are highly reproducible, as summarized in Table 1. Apart from the enhanced efficiency, long-chain BA cations with moisture resistance in the 2D layer (as proven by the water contact angle measurement in Fig. S3, Supporting Information) normally provide the added beneficial effect of improving the 2D/3D PSC lifetime. As shown in Fig. 2c, we studied the long-term stability of PSCs by storing unencapsulated devices in air. After 1000 h, the 2D/3D PSC maintained over 88% of the initial PCE value; by contrast, the efficiency of the pure 3D device rapidly decayed to less than 5% of its original device performance after 384 h. Intuitively, the 2D perovskite capping layer provides gains in both stability and efficiency for the PSC device. Among them, the efficiency improvement is mainly due to the VB levels of the n-value-graded 2D perovskites continuously approaching the VB level of 3D MAPbI_3 [5,14], which finally leads to efficient carrier separation at the 2D/3D interface. From our time-resolved PL (TRPL) decay experimental results in Fig. 2d, the shorter average PL decay lifetime τ of 3.2 ns at the contact between the 2D perovskite and Spiro-OMeTAD further confirms that hole extraction is more efficient than that at the pure 3D perovskite/Spiro-OMeTAD interface ($\tau = 7.2$ ns). Thus, 2D/3D perovskite heterostructures with optimized band alignment can be considered to greatly improve the performance of PSC devices. Nevertheless, TRPL transients cannot provide any information on the local interfacial band structure, which will affect the subsequent 2D/3D PSC optimization.

3.2. Sample preparation for STM

In this study, the combination of STM and scanning tunneling spectroscopy (STS) measurements allows us to reveal the spatially resolved band energy diagrams across 2D/3D perovskite heterointerfaces by analyzing their local electronic density of states (LDOS) [37]. To facilitate the differentiation of interfaces between 2D $(\text{BA})_2(\text{MA})_{n-1}\text{Pb}_n\text{I}_{3n+1}$ and 3D MAPbI_3 during STM manipulation, we synthesized a thicker 2D perovskite capping layer by increasing the concentration of the MAI/BAI-containing isopropanol solution to 50 mM. XTEM results show that the thickness of this STM-specific 2D perovskite overlayer exceeds 100 nm (Fig. S4a, Supporting

Information). Furthermore, both structural (XRD pattern in Fig. S4b, Supporting Information) and optical (PL spectrum in Fig. S4c, Supporting Information) analyses confirmed that the mixed n-value compositions of thick 2D layered perovskites are consistent with that of the thin sample, except for the more 3D-to-2D dimensional reduction. Prior to probing the electronic information across 2D/3D perovskite heterojunctions, how to prepare a clean cross-sectional sample inside STM equipment is a crucial factor affecting the results. Proceeding as we did previously [28], the 2D/3D interface was cleaved in situ at room temperature in an ultrahigh vacuum (UHV) sample preparation chamber with a base pressure of $\sim 5 \times 10^{-11}$ Torr. After applying a force to the perovskite side along the y-axis, as shown in Fig. 3a, a fresh cross-sectional 2D/3D perovskite slice could be immediately obtained, as shown schematically in Fig. 3b. Then, the sample was transferred to an STM operation chamber for further measurement. Fig. 3c presents a topographic 3D cross-sectional STM (XSTM) image of the 2D/3D perovskite heterostructure on ITO glass at a -2.0 V sample bias (V_b) and a fixed tunneling current of 180 pA, where the edges of 2D-capped 3D perovskite grains are marked with gray dashed lines. We further circle a region very close to the grain boundary (i.e., the black dashed rectangle) in Fig. 3c. Usually, 2D perovskite shells grow on the surface of 3D perovskite cores, as in the schematic illustration of the yellow region in Fig. 3c, so this region may cross the 2D/3D perovskite heterostructure. Fig. 3d shows the corresponding magnified XSTM image of the black dashed rectangular region. Two distinctly different height differences are observed on the left (close to the grain boundary) and right (away from the grain boundary) sides of this rectangular region, probably due to the phase mismatch between the 2D and 3D perovskite crystals.

3.3. LM-XSTM measurements

To determine compositional variations on both sides of this height difference, tunneling current maps were generated from XSTM/STS measurements to distinguish the integrated LDOS information for each part within the circled rectangular area. The XSTM operation principle is depicted in Fig. 4a, where a set of tunneling current behaviors can be imaged at various V_b s. Most importantly, once the laser modulation is turned on, real-space monitoring of the photocarrier transfer and photoinduced band bending can be simultaneously achieved through this LM-XSTM technique, as schematically depicted in Fig. 4b. All XSTM and LM-XSTM experiments were carried out at room temperature. Fig. 4c and d show mapping images of the current signals along the

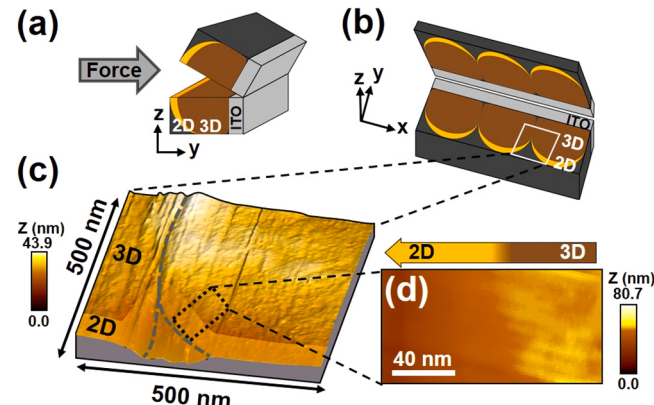


Fig. 3. Cross-sectional sample preparation procedure and corresponding XSTM topography images. Schematic depiction of (a) an essential sample cleaving process and (b) a post-cleaving ITO glass/2D perovskite/3D perovskite film in the XSTM measurement. (c) 3D XSTM topography image recorded at a -2.0 V sample bias of a 2D/3D hybrid perovskite film on an ITO glass substrate. (d) Zoomed-in XSTM topography view of the region in c marked by the black dotted rectangle showing the image edges.

Table 1

Summary of the champion photovoltaic performance parameters and average device characteristics with standard deviation (in brackets) of PSCs for the control pure 3D perovskite-based device and 2D/3D perovskite-based device.

Perovskite structure	V_{OC} (V)	J_{SC} (mA cm^{-2})	FF (%)	PCE (%)
Pure 3D	1.03 (1.02 ± 0.02)	22.73 (22.62 ± 0.24)	73.0 (72.6 ± 1.6)	17.1 (16.8 ± 0.6)
2D/3D	1.08 (1.07 ± 0.01)	23.02 (22.84 ± 0.13)	77.3 (75.9 ± 1.4)	19.2 (18.2 ± 0.7)

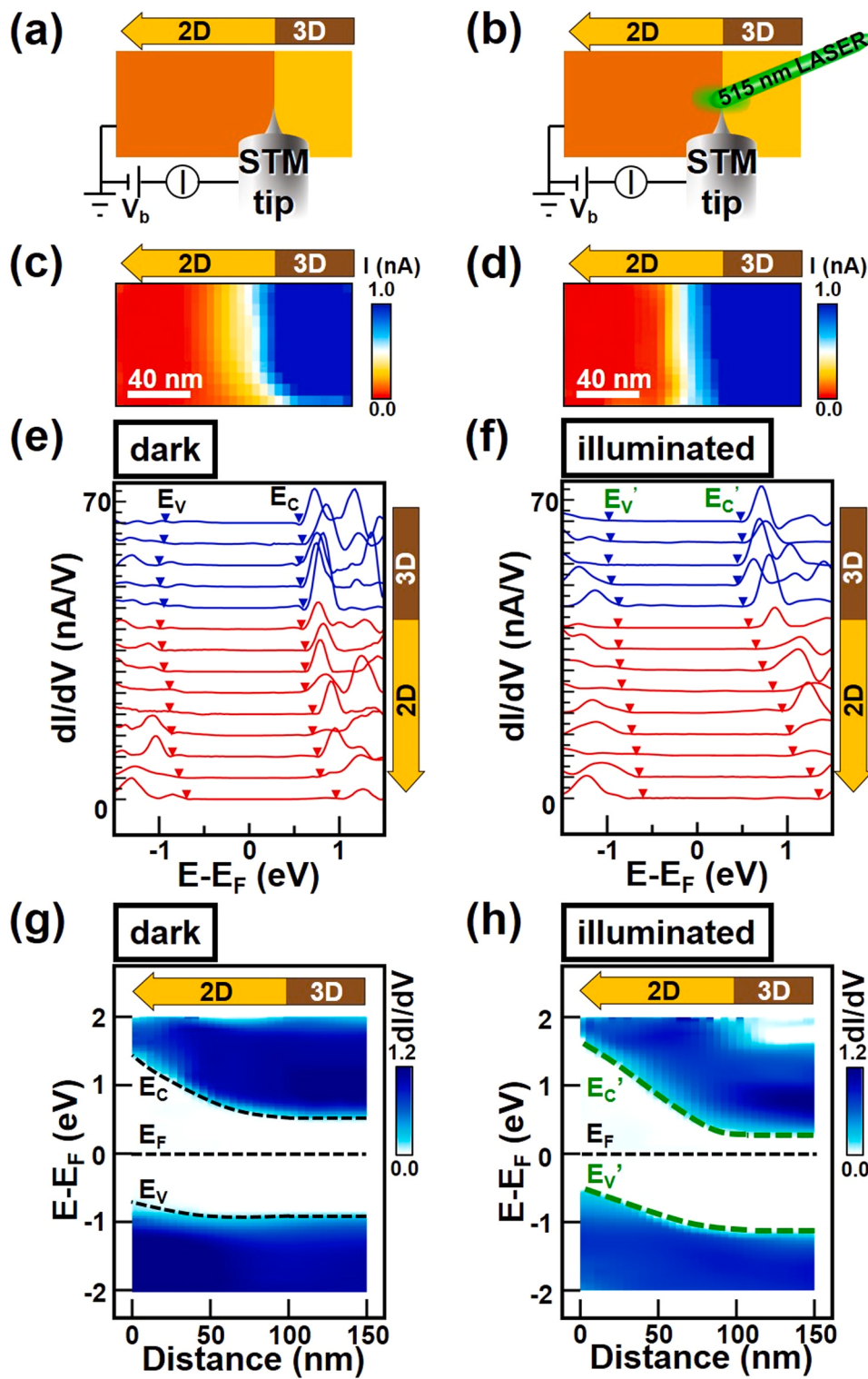


Fig. 4. Monitoring the band alignment across 2D/3D perovskite heterointerfaces using XSTM and LM-XSTM. Schematic illustrations of the XSTM setup (a) in the dark and (b) under 515 nm laser illumination. The sample architecture is ITO glass/2D perovskite/3D perovskite. Mapping images of current spectra across 2D/3D perovskite heterointerfaces probed at a sample bias of +0.8 V (c) in the dark and (d) under 515 nm radiation. Point-to-point evolution of electronic dI/dV curves across 2D perovskite/3D perovskite interfaces (e) in the dark and (f) under 515 nm illumination. Mapping images of the band alignment across 2D/3D perovskite heterointerfaces (g) in the dark and (h) under 515 nm illumination obtained by extracting the positions of the E_C and E_V levels indicated by the inverted triangular marks in e and f, respectively. The scan regions of c-h were the same as those in Fig. 3d.

rectangular region of Fig. 3d obtained at a V_b of +0.8 V by using current imaging tunneling spectroscopy (CITS) mode in the dark and under 515 nm laser illumination, respectively. The CITS results of Fig. 4c show three electronic environments before illumination. The right side (colored blue) has the largest current, the middle region is a transition area (color gradient), and the left side (colored red) has almost no current. The middle region may be the 2D $(BA)_2(MA)_{n-1}Pb_nI_{3n+1}$ perovskites with an n -value gradient, as the electronic properties vary

depending on the n value. The CITS results of Fig. 4d show the same electronic properties on the right and left sides after illumination, whereas the current intensities in the middle vary. The tunneling current values on the right side are mostly larger than those in the middle and on the left side before and after illumination. Moreover, the right side belongs to the region far from the grain boundary (according to the previous morphological observation in Fig. 3d). Combining the high conductivity feature with the location in the grain interior, we infer that

the blue area is composed of the 3D MAPbI_3 perovskite with a small bandgap. By contrast, the poor charge transport 2D $(\text{BA})_2(\text{MA})_{n-1}\text{Pb}_n\text{I}_{3n+1}$ perovskites should be located in the yellow to red gradient and red areas on the left. In addition, the current values clearly vary in the transition area under illumination, demonstrating that the 515 nm laser in LM-XSTM can successfully change the electronic environments induced by photocarriers.

To obtain the vertical band structure across the 2D/3D perovskite heterointerface, Fig. 4e further presents the evolution of some representative dI/dV curves as a function of V_b (equal to $E-E_F$), marked with blue (3D perovskite) and red (2D perovskites) lines. In STM measurements, the Fermi level (E_F) of the sample is at the energy position of zero sample bias. Based on the previous analysis method [38], the positions of dI/dV onsets (marked with inverted triangle symbols) in empty and filled states correspond to CB (equal to E_C) and VB (equal to E_V) edges, respectively. From the topmost dI/dV curve in Fig. 4e, the energy band onsets of the E_C and E_V levels are at approximately 0.59 and -0.93 eV, respectively. The E_C level is closer to the E_F level, which shows the typical n-type feature of MAPbI_3 crystals [39]. Moreover, the bandgap can be calculated as 1.52 eV, which is consistent with the previously reported value of MAPbI_3 [40]. Continuing to explore the rest of the blue section, we found that the CB and VB edges are nearly identical, further confirming that this is the region of the unmodified 3D perovskite. Afterward, the 2D perovskite region was scanned sequentially toward the grain boundary. At the outermost 2D perovskite part (i.e., the bottom curve of Fig. 4e), the onset biases of the E_C and E_V levels are located at 0.96 and -0.70 eV, respectively, resulting in a bandgap of 1.66 eV. This value is consistent with the bandgap of the 2D perovskite $(\text{BA})_2(\text{MA})_4\text{Pb}_5\text{I}_{16}$ ($n = 5$) [40]. In addition, both the CB and VB edges shift to a high sample bias position step-by-step when scanning from the interior of the 2D perovskite to the surface. Among them, the displacement of the CB edge is larger than that of the VB edge. Thus, spontaneous formation of a gradually increased bandgap along the 2D perovskite-to-grain boundary direction is found. Based on this spatially dependent electronic information, Fig. 4g plots a mapping image of the band alignment across the 2D/3D perovskite heterojunction. The offsets of the E_C and E_V levels from the interior to outer 2D perovskites are approximately 0.38 and 0.26 eV, respectively. As a result, these unbalanced energy band edge transitions lead to the 2D perovskites exhibiting progressively enhanced hole-conducting (p-type) semiconductor properties from the inside out. Accordingly, this resultant mapping diagram with continuously upshifting band edges visually shows that hole extraction is accelerated by inserting the 2D overlayer into the interface between the Spiro-OMeTAD hole transporter and the 3D perovskite.

Next, we used the LM-XSTM technique for direct visualization of spatially resolved dI/dV signals across 2D/3D perovskites under 515 nm laser illumination. In this work, the CB and VB edges after illumination are denoted by the E_C' and E_V' levels, respectively. As shown in Fig. 4f, all E_C' and E_V' levels of the 3D perovskite and the region close to the 2D/3D perovskite interface are shifted downward after illumination, and E_C' is close to the E_F level. By contrast, the energy bands in the 2D perovskite part away from the interface are shifted in the opposite direction after illumination. These photoinduced changes in the band alignment are summarized in a mapping image. Fig. 4h demonstrates the real-space band alignment across the 2D/3D perovskite p-n junction under illumination. The bending level in the 2D region is clearly much larger after illumination. That is, the potential energy between the interface and away from the interface increases in the 2D region. The electric field in the 2D region is enhanced after photodoping. After that, a more efficient photocarrier separation/transfer process occurs across the 2D/3D perovskites. To the best of our knowledge, this is the first time the combination of cross-sectional and light-modulation technologies has been used to plot the interfacial band diagram of perovskite devices, and subsequently, this measurement could be extended to other semiconductor systems.

3.4. Impact of 2D/3D perovskite heterojunctions on PSCs

To gain more insight into the mechanism of the 2D-capped 3D perovskite heterojunction in improving the PSC performance, we performed photocarrier dynamic studies based on the above visualized dI/dV spectra. Fig. 5a presents the average normalized dI/dV curves of the 3D perovskite in the dark and under illumination. The energy differences (E_D) between the E_C level and the E_F level, defined as $E_D = E_C - E_F$, can be used to evaluate the carrier concentration in addition to determining the carrier type of the semiconductor [29]. To highlight the distinction, the energy difference under illumination is denoted as E_D' . In Fig. 5a, the open blue triangle symbol shifts toward the solid blue triangle symbol after 515 nm laser irradiation, and finally, the E_D value is reduced to E_D' . This shows that photoinduced n-type doping occurs in the light-sensitive 3D perovskite crystal. Moreover, after light illumination, slight LDOS enhancements are noted from the dI/dV curves regardless of a positive or negative sample bias. This variation is due to the enhancement of the tunneling current from the CB (or VB) edge to the STM tip, which corresponds to an increase in the carrier density of photogenerated electrons (or holes) in the 3D perovskite. In the 2D counterpart (the measurement here is approximately 60 nm from the 2D/3D interface), E_C moves to a higher energy position (that is, the open red triangle symbol shifts toward the solid red triangle symbol), and finally, the E_D value is increased to E_D' , as illustrated in Fig. 5b. Apparently, this is a p-type photodoping behavior. More particularly, a significant enhancement of the LDOS is found from the dI/dV spectra. This result indicates that the carrier density in the 2D perovskites is greatly increased after illumination. Fig. 5c and d show the spatial distributions of the energy differences obtained from the 2D/3D perovskites without and with laser illumination, respectively, where the E_D and E_D' values were collected from the individual normalized dI/dV signals. Based on Fig. 5c and d, the E_D and E_D' approach constant values in the 3D region and show a gradient distribution from the interface in the 2D region. Therefore, the mapping images of E_D and E_D' values correlate with the dimensional distribution of 3D MAPbI_3 and 2D $(\text{BA})_2(\text{MA})_{n-1}\text{Pb}_n\text{I}_{3n+1}$. Comparing these two spectra, the E_D values in the 3D region and the 2D area away from the interface decrease and increase under illumination, respectively. This visualized photocarrier flow is due to the establishment of a new series of energy bands across the 2D/3D perovskite heterojunction, which leads to promotion of the charge carrier generation, separation and transport behaviors. Next, the variation in the energy difference (ΔE_D), denoted as $\Delta E_D = E_D' - E_D$, can be plotted as an image to directly observe the distribution of the carrier concentration and the transition of the semiconductor type across the 2D/3D perovskites. Fig. 5e shows a mapping result of the real-space distributed ΔE_D values monitored in 2D/3D crystals after illumination. Most of the ΔE_D values in the 3D part and the 2D region near the interface are negative (colored light blue), whereas they are positive in the 2D area away from the interface (colored orange). Obviously, the mapping image of ΔE_D values away from the interface implies that the photoexcited charge transfer behavior strongly depends on the composition of the perovskites. In detail, photogenerated excitons will be induced inside the 2D/3D perovskites after exposure to a laser. Then, the excitons will drift and be separated at the 2D/3D perovskite heterointerface. The negative ΔE_D values are the result of the photogenerated electron-rich regions in MAPbI_3 and the nearby interface. At the same time, the remaining photoinduced holes in the 3D perovskite will drift and be effectively transported to the 2D part by the continuously upshifting VB edges. Therefore, hole-rich regions form throughout the 2D perovskite region away from the interface.

3.5. Band structure

Fig. 6a and b summarize the interfacial band structure across the 2D/3D perovskites in the dark and under laser illumination, respectively, according to the previously plotted band alignments and corresponding

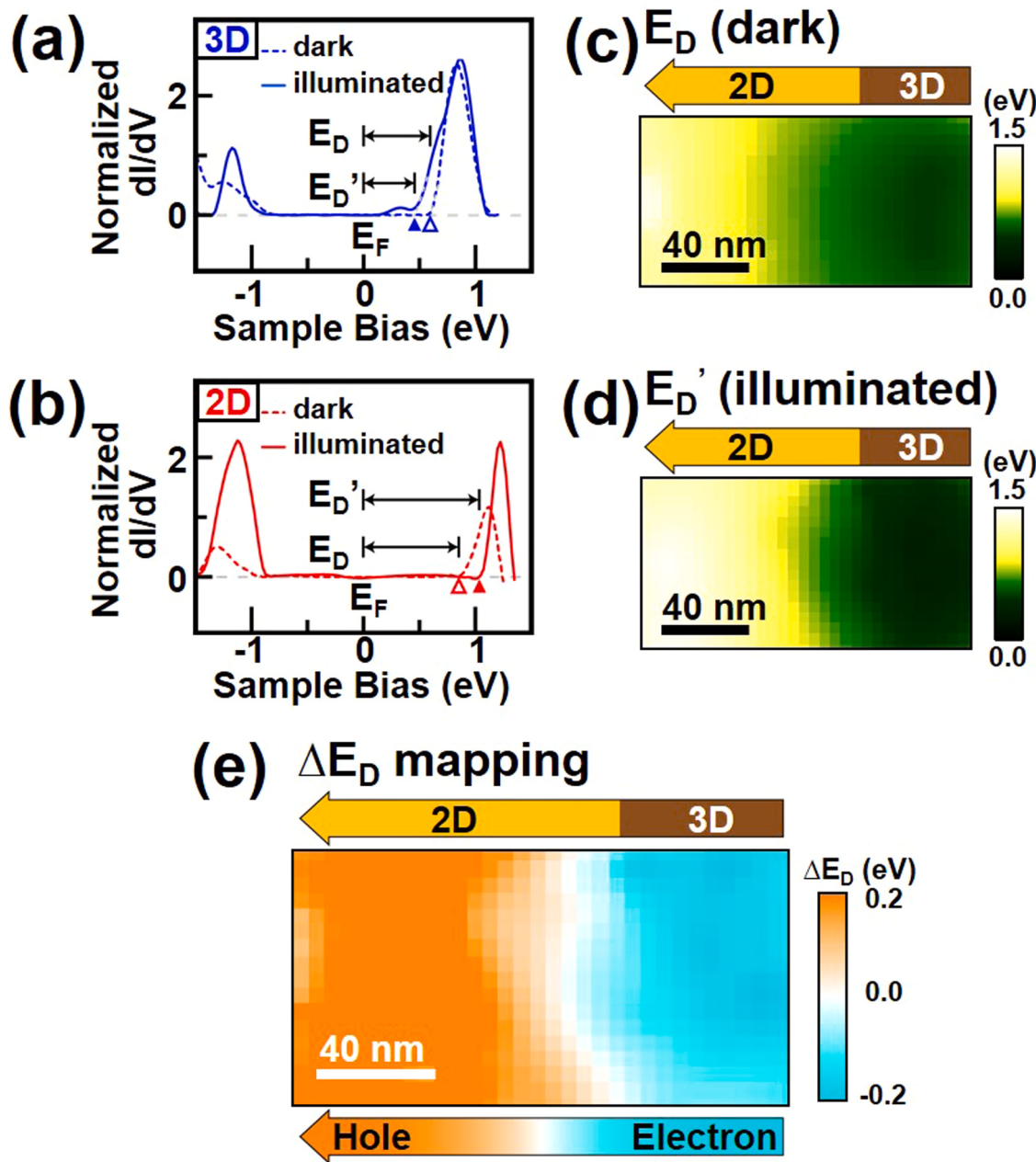


Fig. 5. Photocarrier dynamics. Representative normalized dI/dV signals of the (a) 3D perovskite and (b) 2D perovskites in the dark (dotted curve) and under 515 nm illumination (solid curve). Imaging of spatial distributions of (c) E_D values (in the dark) and (d) E_D' values (under 515 nm radiation) observed from the 2D/3D perovskite heterostructure. (e) Mapping image of the distribution of ΔE_D values ($\Delta E_D = E_D' - E_D$) derived from the 2D/3D perovskite heterointerface.

ΔE_D analysis. As mentioned earlier, a series of continuously upshifting bands appears in the 2D layers due to their n-value gradient, which is consistent with Fig. 6a. After illumination, the energy band of the 2D perovskites away from the interface is bent more upward, and that of the 2D perovskites at the interface is bent downward, which indicates that the electric field increases in the 2D region. As a result of the more upward bending energy band structure, the photoexcited holes in the 3D perovskite more readily drift into the 2D overlayer, thus limiting electron transport to the 2D region. That is, the excitons are more easily separated at this tailored 2D/3D interface under illumination, ultimately reducing electron-hole recombination. Subsequently, higher concentrations of electrons and holes are collected in each of the 3D and 2D perovskites through this improved band structure (referring to the process from Fig. S5a–b, Supporting Information). Theoretically, the increase in hole concentrations in the 2D perovskites corresponds to the

hole quasi-Fermi level (E_{Fp}) approaching the VB edge, and the increase in the electron concentration in the 3D perovskite corresponds to the electron quasi-Fermi level (E_{Fn}) approaching the CB edge (Fig. S5b, Supporting Information). To match the energy levels of the electron/hole transport layers, the band structure is spontaneously adjusted, leading to a downshifted E_{Fp} and an upshifted E_{Fn} [15]. After equilibrium is reached, the photoinduced band edges (including E_C' and E_V') in the 2D perovskites away from the interface are shifted to higher energy levels, and conversely, the band edges in the 3D perovskite are shifted to lower energy levels (Fig. 6b). Finally, this phenomenon enhances the electric field in the 2D perovskites, facilitating the separation of carriers. These results show that the LM-XSTM measurement provides a visual solution for determining the operational mechanisms of 2D/3D PSCs, which will be beneficial for future PSC performance optimization.

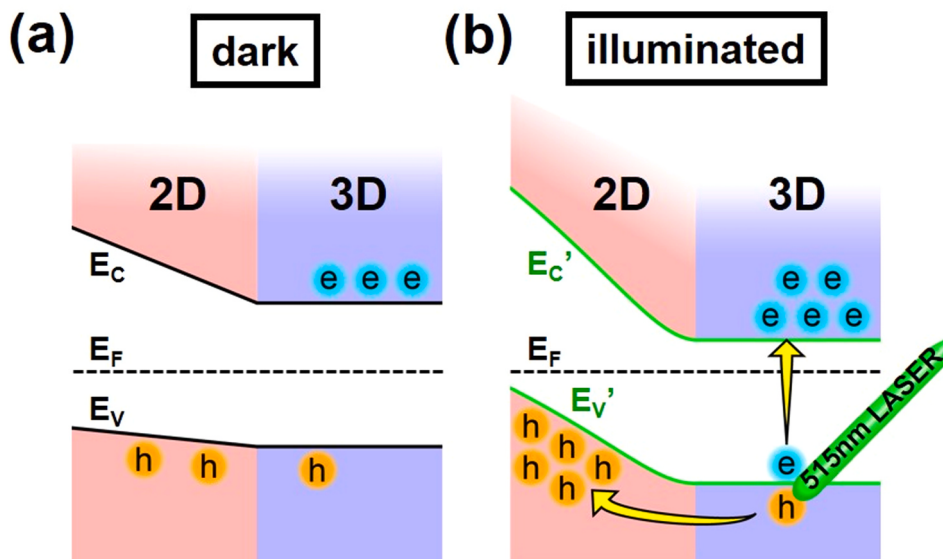


Fig. 6. Band diagrams. Schematic energy level diagrams across the 2D/3D perovskites (a) in the dark and (b) under 515 nm illumination.

4. Conclusion

In conclusion, we show real-space visualization of the interfacial band alignment and photocarrier distribution across 2D-capped 3D perovskite heterostructures using the LM-XSTM technique. This observation reveals that the 2D perovskite overlayer can accelerate the extraction of holes from the 3D perovskite light harvester due to the existence of a photoenhanced electric field, and it can also assist hole transport to the hole transporter through its gradient upshifting energy levels. This state-of-the-art LM-XSTM technology allows us to identify and improve the PSC device performance by understanding the local operating mechanism, and it is also highly compatible with other semiconductor devices.

CRediT authorship contribution statement

C.-W.C., Y.-P.C. and Y.-C.W. conceived and supervised the study. **P.-C.H., M.-C.S. and C.-H.C.** performed the STM experiments. **S.-K.H., T.-C.L., C.-C.L. and C.-Y.L.** fabricated the 2D/3D perovskite crystals and optimized the solar cell performance. **P.-C.H., S.-K.H., M.-C.S., H.-C.H., C.-H.C. and Y.-C.W.** conducted the data collection, interpretation and analysis. **C.-W.C., Y.-P.C., K.T., S.-F.T. and Y.-C.W.** wrote and revised the manuscript. All authors agreed to the manuscript content.

Declaration of Competing Interest

The authors declare that they have no known competing financial interests or personal relationships that could have appeared to influence the work reported in this paper.

Acknowledgements

Y.-C.W. acknowledges the financial support from JSPS-KAKENHI (Grant No. 20K15135) and the ICYS, NIMS for the research funds. **C.-W.C.** acknowledges the financial support from the Ministry of Science and Technology (MOST), Taiwan (Contract No. MOST 108-2923-M-002-002-MY2, MOST-NIMS add-on project). **Y.-P.C.** acknowledges the financial support from the Ministry of Science and Technology (MOST), Taiwan (Contract No. MOST 109-2628-M-002-005-MY3) and National Taiwan Univ. (Contract No. NTU-109L7848). Financial support provided by the Center of Atomic Initiative for New Materials (AI-Mat), National Taiwan University, from the Featured Areas Research Center

Program within the framework of the Higher Education Sprout Project by the Ministry of Education in Taiwan (Grant No. 108L9008) is also acknowledged.

Appendix A. Supporting information

Supplementary data associated with this article can be found in the online version at doi:10.1016/j.nanoen.2021.106362.

References

- [1] J.Y. Kim, J.-W. Lee, H.S. Jung, H. Shin, N.-G. Park, High-efficiency perovskite solar cells, *Chem. Rev.* 120 (2020) 7867–7918.
- [2] L. Chouhan, S. Ghimire, C. Subrahmanyam, T. Miyasaka, V. Biju, Synthesis, optoelectronic properties and applications of halide perovskites, *Chem. Soc. Rev.* 49 (2020) 2869–2885.
- [3] H. Sun, K. Deng, J. Xiong, L. Li, Graded bandgap perovskite with intrinsic n-p homojunction expands photon harvesting range and enables all transport layer-free perovskite solar cells, *Adv. Energy Mater.* 10 (2020), 1903347.
- [4] B. Shi, L. Duan, Y. Zhao, J. Luo, X. Zhang, Semitransparent perovskite solar cells: from materials and devices to applications, *Adv. Mater.* 32 (2020), 1806474.
- [5] T. Zhang, M. Long, M. Qin, X. Lu, S. Chen, F. Xie, L. Gong, J. Chen, M. Chu, Q. Miao, Z. Chen, W. Xu, P. Liu, W. Xie, J.-b Xu, Stable and efficient 3D-2D perovskite-perovskite planar heterojunction solar cell without organic hole transport layer, *Joule* 2 (2018) 2706–2721.
- [6] Y.-C. Wang, S.-K. Huang, T. Nakamura, Y.-T. Kao, C.-H. Chiang, D.-Y. Wang, Y. J. Chang, N. Koshida, T. Shimada, S. Liu, C.-W. Chen, K. Tsukagoshi, Quantum-assisted photoelectric gain shifts in perovskite solar cells, *NPG Asia Mater.* 12 (2020) 54.
- [7] G.E. Eperon, S.D. Stranks, C. Menelaou, M.B. Johnston, L.M. Herz, H.J. Snaith, Formamidinium lead trihalide: a broadly tunable perovskite for efficient planar heterojunction solar cells, *Energy Environ. Sci.* 7 (2014) 982–988.
- [8] G. Xing, N. Mathews, S. Sun, S.S. Lim, Y.M. Lam, M. Grätzel, S. Mhaisalkar, T. C. Sum, Long-range balanced electron- and hole-transport lengths in organic-inorganic $\text{CH}_3\text{NH}_3\text{PbI}_3$, *Science* 342 (2013) 344–347.
- [9] A. Kojima, K. Teshima, Y. Shirai, T. Miyasaka, Organometal halide perovskites as visible-light sensitizers for photovoltaic cells, *J. Am. Chem. Soc.* 131 (2009) 6050–6051.
- [10] NREL, (<https://www.nrel.gov/pv/cell-efficiency.html>).
- [11] W. Huang, T. Bu, F. Huang, Y.-B. Cheng, Stabilizing high efficiency perovskite solar cells with 3D-2D heterostructures, *Joule* 4 (2020) 975–979.
- [12] Z. Fang, M. Shang, Y. Zheng, T. Zhang, Z. Du, G. Wang, X. Duan, K.-C. Chou, C.-H. Lin, W. Yang, X. Hou, T. Wu, Organic intercalation engineering of quasi-2D Dion-Jacobson $\alpha\text{-CsPbI}_3$ perovskites, *Mater. Horiz.* 7 (2020) 1042–1050.
- [13] G. Grancini, C. Roldán-Carmona, I. Zimmermann, E. Mosconi, X. Lee, D. Martineau, S. Narbey, F. Oswald, F.D. Angelis, M. Graetzel, M.K. Nazeeruddin, One-year stable perovskite solar cells by 2D/3D interface engineering, *Nat. Commun.* 8 (2017) 15684.
- [14] Y. Bai, S. Xiao, C. Hu, T. Zhang, X. Meng, H. Lin, Y. Yang, S. Yang, Dimensional engineering of a graded 3D-2D halide perovskite interface enables ultrahigh V_{oc} enhanced stability in the p-i-n photovoltaics, *Adv. Energy Mater.* 7 (2017), 1701038.

- [15] P. Chen, Y. Bai, S. Wang, M. Lyu, J.H. Yun, L. Wang, In situ growth of 2D perovskite capping layer for stable and efficient perovskite solar cells, *Adv. Funct. Mater.* 28 (2018), 1706923.
- [16] A.H. Proppe, M. Wei, B. Chen, R. Quintero-Bermudez, S.O. Kelley, E.H. Sargent, Photochemically cross-linked quantum well ligands for 2D/3D perovskite photovoltaics with improved photovoltage and stability, *J. Am. Chem. Soc.* 141 (2019) 14180–14189.
- [17] M.-G. La-Placa, L. Gil-Escrí, D. Guo, F. Palazon, T.J. Savenije, M. Sessolo, H. J. Bolink, Vacuum-deposited 2D/3D perovskite heterojunctions, *ACS Energy Lett.* 4 (2019) 2893–2901.
- [18] B. Liu, M. Long, M. Cai, L. Ding, J. Yang, Interfacial charge behavior modulation in 2D/3D perovskite heterostructure for potential high-performance solar cells, *Nano Energy* 59 (2019) 715–720.
- [19] S. Gharibzadeh, B.A. Nejand, M. Jakoby, T. Abzieher, D. Hauschild, S. Moghadamzadeh, J.A. Schwenzer, P. Brenner, R. Schmager, A.A. Haghhighirad, L. Weinhardt, U. Lemmer, B.S. Richards, I.A. Howard, U.W. Paetzold, Record open-circuit voltage wide-bandgap perovskite solar cells utilizing 2D/3D perovskite heterostructure, *Adv. Energy Mater.* 9 (2019), 1803699.
- [20] Q. Yao, Q. Xue, Z. Li, K. Zhang, T. Zhang, N. Li, S. Yang, C.J. Brabec, H.L. Yip, Y. Cao, Graded 2D/3D perovskite heterostructure for efficient and operationally stable MA-free perovskite solar cells, *Adv. Mater.* 32 (2020), 2000571.
- [21] A.A. Sutanto, R. Szostak, N. Drigo, V.I.E. Queloz, P.E. Marchezi, J.C. Germino, H.C. N. Tolentino, M.K. Nazeeruddin, A.F. Nogueira, G. Grancini, In situ analysis reveals the role of 2D perovskite in preventing thermal-induced degradation in 2D/3D perovskite interfaces, *Nano Lett.* 20 (2020) 3992–3998.
- [22] Y. Liu, S. Akin, A. Hinderhofer, F.T. Eickemeyer, H. Zhu, J.Y. Seo, J. Zhang, F. Schreiber, H. Zhang, S.M. Zakeeruddin, A. Hagfeldt, M.I. Dar, M. Grätzel, Stabilization of highly efficient and stable phase-pure FAPbI₃ perovskite solar cells by molecularly tailored 2D-overlayers, *Angew. Chem. Int. Ed.* 59 (2020) 15688–15694.
- [23] H. Tsai, W. Nie, J.-C. Blancon, C.C. Stoumpos, R. Asadpour, B. Harutyunyan, A. J. Neukirch, R. Verduzco, J.J. Crochet, S. Tretiak, L. Pedesseau, J. Even, M. A. Alam, G. Gupta, J. Lou, P.M. Ajayan, M.J. Bedzyk, M.G. Kanatzidis, A.D. Mohite, High-efficiency two-dimensional Ruddlesden-Popper perovskite solar cells, *Nature* 536 (2016) 312–316.
- [24] Z. Wang, Q. Lin, F.P. Chmiel, N. Sakai, L.M. Herz, H.J. Snaith, Efficient ambient-air-stable solar cells with 2D–3D heterostructured butylammonium-caesium-formamidinium lead halide perovskites, *Nat. Energy* 2 (2017) 17135.
- [25] J.-W. Lee, Z. Dai, T.-H. Han, C. Choi, S.-Y. Chang, S.-J. Lee, N.D. Marco, H. Zhao, P. Sun, Y. Huang, Y. Yang, 2D perovskite stabilized phase-pure formamidinium perovskite solar cells, *Nat. Commun.* 9 (2018) 3021.
- [26] H. Ren, S. Yu, L. Chao, Y. Xia, Y. Sun, S. Zuo, F. Li, T. Niu, Y. Yang, H. Ju, B. Li, H. Du, X. Gao, J. Zhang, J. Wang, L. Zhang, Y. Chen, W. Huang, Efficient and stable Ruddlesden-Popper perovskite solar cell with tailored interlayer molecular interaction, *Nat. Photonics* 14 (2020) 154–163.
- [27] B.-C. Huang, Y.-P. Chiu, P.-C. Huang, W.-C. Wang, V.T. Tra, J.-C. Yang, Q. He, J.-Y. Lin, C.-S. Chang, Y.-H. Chu, Mapping band alignment across complex oxide heterointerfaces, *Phys. Rev. Lett.* 109 (2012), 246807.
- [28] M.-C. Shih, B.-C. Huang, C.-C. Lin, S.-S. Li, H.-A. Chen, Y.-P. Chiu, C.-W. Chen, Atomic-scale interfacial band mapping across vertically phased-separated polymer/fullerene hybrid solar cells, *Nano Lett.* 13 (2013) 2387–2392.
- [29] M.-C. Shih, S.-S. Li, C.-H. Hsieh, Y.-C. Wang, H.-D. Yang, Y.-P. Chiu, C.-S. Chang, C.-W. Chen, Spatially resolved imaging on photocarrier generations and band alignments at perovskite/PbI₂ heterointerfaces of perovskite solar cells by light-modulated scanning tunneling microscopy, *Nano Lett.* 17 (2017) 1154–1160.
- [30] J.-C. Lin, V.T. Tra, D.-S. Tsai, T.-T. Lin, P.-C. Huang, W.-L. Hsu, H.J. Wu, R. Huang, N.V. Chien, R. Yoshida, J.-Y. Lin, Y. Ikuhara, Y.-P. Chiu, S. Gwo, D.P. Tsai, J.-H. He, Y.-H. Chu, Control of the metal–insulator transition at complex oxide heterointerfaces through visible light, *Adv. Mater.* 28 (2016) 764–770.
- [31] F.-M. Hsiao, M. Schnedler, V. Portz, Y.-C. Huang, B.-C. Huang, M.-C. Shih, C.-W. Chang, L.-W. Tu, H. Eisele, R.E. Dunin-Borkowski, P. Ebert, Y.-P. Chiu, Probing defect states in polycrystalline GaN grown on Si(111) by sub-bandgap laser-excited scanning tunneling spectroscopy, *J. Appl. Phys.* 121 (2017), 015701.
- [32] S.-K. Huang, Y.-C. Wang, W.-C. Ke, Y.-T. Kao, N.-Z. She, J.-X. Li, C.-W. Luo, A. Yabushita, D.-Y. Wang, Y.J. Chang, K. Tsukagoshi, C.-W. Chen, Unravelling the origin of the photocarrier dynamics of fullerene-derivative passivation of SnO₂ electron transporters in perovskite solar cells, *J. Mater. Chem. A* 8 (2020) 23607–23616.
- [33] L. Li, N. Zhou, Q. Chen, Q. Shang, Q. Zhang, X. Wang, H. Zhou, Unraveling the growth of hierarchical quasi-2D/3D perovskite and carrier dynamics, *J. Phys. Chem. Lett.* 9 (2018) 1124–1132.
- [34] C.M. Raghavan, T.-P. Chen, S.-S. Li, W.-L. Chen, C.-Y. Lo, Y.-M. Liao, G. Haider, C.-C. Lin, C.-C. Chen, R. Sankar, Y.-M. Chang, F.-C. Chou, C.-W. Chen, Low-threshold lasing from 2D homologous organic–inorganic hybrid Ruddlesden-Popper perovskite single crystals, *Nano Lett.* 18 (2018) 3221–3228.
- [35] C.C. Stoumpos, D.H. Cao, D.J. Clark, J. Young, J.M. Rondinelli, J.I. Jang, J. T. Hupp, M.G. Kanatzidis, Ruddlesden-Popper hybrid lead iodide perovskite 2D homologous semiconductors, *Chem. Mater.* 28 (2016) 2852–2867.
- [36] Y.C. Wang, X. Li, L. Zhu, X. Liu, W. Zhang, J. Fang, Efficient and hysteresis-free perovskite solar cells based on a solution processable polar fullerene electron transport layer, *Adv. Energy Mater.* 7 (2017), 1701144.
- [37] R. Ohmann, L.K. Ono, H.-S. Kim, H. Lin, M.V. Lee, Y. Li, N.-G. Park, Y. Qi, Real-space imaging of the atomic structure of organic–inorganic perovskite, *J. Am. Chem. Soc.* 137 (2015) 16049–16054.
- [38] R.M. Feenstra, Tunneling spectroscopy of the (110) surface of direct-gap III-V semiconductors, *Phys. Rev. B Condens. Matter Mater. Phys.* 50 (1994) 4561–4570.
- [39] Q. Wang, Y. Shao, H. Xie, L. Lyu, Y. Gao, J. Huang, Qualifying composition dependent p and n self-doping in CH₃NH₃PbI₃, *Appl. Phys. Lett.* 105 (2014), 163508.
- [40] C.M.M. Soe, G.P. Nagabhushana, R. Shivaramaiah, H. Tsai, W. Nie, J.-C. Blancon, F. Melkonyan, D.H. Cao, B. Traoré, L. Pedesseau, M. Kepenekian, C. Katan, J. Even, T.J. Marks, A. Navrotsky, A.D. Mohite, C.C. Stoumpos, M.G. Kanatzidis, Structural and thermodynamic limits of layer thickness in 2D halide perovskites, *Proc. Natl. Acad. Sci. USA* 116 (2019) 58–66.



Po-Cheng Huang received his M.S. degree in 2012 from Department of Physics, National Sun Yat-sen University in Taiwan. He studied his Ph.D. student in 2012–2018 at Department of Physics, National Sun Yat-sen University. He currently works as a Research and Development Substitute Services at the Department of Physics, National Taiwan University. His research is focus on the interfacial physics of the perovskite materials.



Shao-Ku Huang received the B.S. degree and M.S. degree in the Department of Physics at the Tamkang University. He obtained his Ph.D. degree in the Department of Materials Science and Engineering at the National Taiwan University under the supervision of Prof. Chun-Wei Chen from 2016 to 2021. His research focuses on organic-inorganic hybrid perovskite application and Density Functional Theory (DFT) simulation.



Ting-Chun Lai received the B.S. degree in 2016 from National Chiao Tung University and the M.S. degree in Material Science in 2018 from National Taiwan University. She is currently an engineer in research and development department in Chang Chun Petrochemical Co., Ltd. Her main research interests focus on perovskite materials and their photovoltaic applications.



Min-Chuan Shih received his Ph.D. degree in 2016 from Department of Physics, National Sun Yat-sen University in Taiwan. He received an award of the “Postgraduates Student Thesis Award from the Physical Society of Republic of China” in 2016. Afterwards, he worked as a postdoctoral researcher at the Department of Physics, National Taiwan University from 2016 to 2020. His research is focus on the physics of the polymer-based and perovskite-based solar cells. He studied the light-modulated scanning tunneling microscopy experiment technique with the solar cells and semiconductor.



Hung-Chang Hsu received his Ph.D. degree in 2016 from Department of Physics, National Taiwan Normal University. He is currently a postdoctoral researcher at the Department of Physics, National Taiwan University. He received an award of the "Ministry of Science and Technology (MOST) Postdoctoral Researcher Academic Research Award Awardees" in 2019. His research is focus on the interfacial science of the semiconductor and the solar cells.



Kazuhito Tsukagoshi studied experimental research on transport physics in semiconductor microstructure and completed his Ph.D. (Osaka University) in 1995. After that he worked as a visiting associate in Cavendish laboratory (University of Cambridge, U.K.) and then in Hitachi Cambridge Laboratory (Hitachi Europe Ltd, U.K.). In 1999, he joined RIKEN where he carried out research on functional thin-film electronics. He continued this research in AIST in 2008, and moved to NIMS in 2009. His current research focuses on nano-material applications for nano-electronics.



Chun-Hsiang Chen received his M.S. degree in 2016 from Department of Physics, National Sun Yat-sen University in Taiwan. He studied his Ph.D. student and worked as a Research and Development Substitute Services in 2016–2019 at the Department of Physics, National Taiwan University. His research is focus on the physics of the solar cells and Graphene.



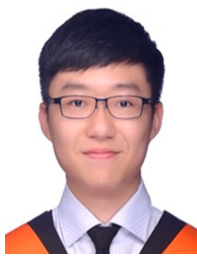
Prof. Chun-Wei Chen received his B.S. degree in National Taiwan University (NTU), Taiwan (1993) and M. Phil (1995) and Ph.D. (1998) degrees from Cambridge University, U.K. He joined the faculty of Department of Materials Science and Engineering, NTU in 2002, where he is currently a Distinguished Professor. His major research interests include the development of next-generation energy materials. He also has extensive research activities on graphene and two-dimensional (2D) materials. He is a recipient of Outstanding Researcher Award (2011 and 2015) from Ministry of Science and Technology, Taiwan and Outstanding Scholar Awards, Foundation for the Advancement of Outstanding Scholarship (2017).



Cheng-Chieh Lin is currently a Ph.D. student in the International Graduate Program of Molecular Science and Technology at National Taiwan University (NTU-MST). He received his M. Sc. degree in 2018 from National Taiwan Normal University. His research interests have focused on the development of hybrid perovskite materials and their application for optoelectronic devices and photocatalysts.



Prof. Ya-Ping Chiu is currently a professor in Department of Physics, National Taiwan University. Her received awards of the "Academia Sinica Early-Career Investigator Research Achievement Award" and "L'ORÉAL-UNESCO Awards for Women in Science" in 2015. Her research interest is in the field of surface science by using scanning tunneling microscopy (STM). In addition, her research works also use the capability of cross-sectional STM to study the interfacial property in semiconductors, complex oxides, and to explore the interlayer property in superconductors.



Chun-Hao Chiang received his B.S. degree in the Department of Materials Science and Engineering from National Taiwan University, Taiwan in 2019. He is currently a Ph.D. candidate under the supervision of Prof. Chun-Wei Chen in National Taiwan University. His doctoral research is mainly focused on the optoelectronic properties and devices of nanomaterials in energy-related fields.



Prof. Shio-w Fon Tsay is currently a distinguished professor in Department of Physics, National Sun Yat-sen University in Taiwan. Her received several awards from "Marquis Who's Who" and received "Albert Nelson Marquis Lifetime Achievement Award" in 2017. Her research is focus on the Superconductivity Physics, Computational Physics, Condensed Matter Physics, and Surface Physics.



Chi-Ying Lin is currently a Ph.D. student in National Taiwan University. He received his master degree in Material Science and Engineering in 2021 from National Taiwan University. His research interests have focused on the perovskite solar cell and magneto-optical semiconductor.



Ying-Chiao Wang is currently an ICYS Research Fellow at International Center for Young Scientists (ICYS), National Institute for Materials Science (NIMS). He pursued his Ph.D. from National Taiwan University in the area of Material Science in 2015. Afterwards he joined distinguished young researcher position at the Ningbo Institute of Material Technology & Engineering, Chinese Academy of Sciences from 2016 to 2018. After that, he worked as a postdoctoral researcher at the Department of Electrical Engineering and Computer Science, School of Engineering, Nagoya University in 2018. His research interests have focused on the development of solution-processed nanomaterials and their photovoltaic applications.